Journal of Geodynamics 65 (2013) 218–227

Contents lists available at SciVerse ScienceDirect

Journal of Geodynamics

journal homepage: http://www.elsevier.com/locate/jog

Application of GPR to normal faults in the Büyük Menderes Graben, western Turkey

Cahit Çağlar Yalçıner[a,*], Erhan Altunel[b], Maksim Bano[c], Mustapha Meghraoui[c], Volkan Karabacak[b], H. Serdar Akyüz[d]

[a] Çanakkale Onsekiz Mart University, Department of Geophysics Engineering, Çanakkale, Turkey
[b] Eskişehir Osmangazi University, Department of Geological Engineering, Eskişehir, Turkey
[c] EOST – CNRS UMR 7516, 5 rue René Descartes, 67084 Strasbourg Cedex, France
[d] İstanbul Technical University, Department of Geology Engineering, Turkey

ARTICLE INFO

Article history:
Received 1 November 2011
Received in revised form 19 May 2012
Accepted 21 May 2012
Available online 29 May 2012

Keywords:
Ground penetrating radar (GPR)
Active faults
Surface ruptures
Trenching

ABSTRACT

Paleoseismology documents past surface-rupturing earthquakes that occurred on faults. This study is limited by the scarcity data on geomorphic and sedimentary environments that may preserve adequate records of deposition, erosion, and fault slip markers. Identifying relevant trenching sites can be difficult when a fault is buried or its surface expression has been eroded since the last tectonic motion. Ground penetrating radar (GPR) is an effective tool for locating suitable sites for trenching. Characteristic reflections are produced by boundaries between elements with contrasting electrical properties, such as grain size distribution (sorting, clay content, etc.), porosity, and water content. GPR is capable of resolving faults by imaging offset stratigraphic reflectors or reflections from the fault plane. GPR surveys were performed at two sites along the Büyük Menderes Graben (western Turkey) to precisely locate the normal fault zone; there is no clear evidence of surface rupture at these sites. We used 250 and 500 MHz antennas for receiving the GPR data. From the GPR measurements, we determined locations suitable for paleoseismic investigations and performed a trenching study across the fault plane. The comparison of the GPR results and the trenching study indicates a good correlation between these methods.

1. Introduction

Ground penetrating radar (GPR) is a shallow geophysical survey technique used to identify underground bodies and structures by digitally identifying changes in electromagnetic signals. The technique is based on the propagation, reflection, and scattering of high-frequency (10 MHz to 2 GHz) electromagnetic (EM) waves in the subsurface (Davis and Annan, 1989; Daniels, 2004). This method has been successfully applied in different disciplines such as archeology (e.g., Leckebusch, 2003; Conyers, 2004; Leucci and Negri, 2006; Yalçıner et al., 2009), geophysics (e.g., Annan et al., 1975; Jol, 1995; Bano et al., 2000), and geology (e.g., Meghraoui et al., 2001; Audru et al., 2001; Gross et al., 2002; Green et al., 2003; Ferry et al., 2004; Malik et al., 2007, and Christie et al., 2009) to investigate buried features. In addition, it has been used in contaminated land, forensic, and snow and ice investigations (e.g., Lalumiere, 2000, 2006; Scambos and Bauer, 2006; Bano et al., 2009). New types of shielded GPR antennas provide more rapid and reliable results with high resolution; however, from the viewpoint of the usefulness of the GPR data, the following parameters must be taken into consideration – the thickness of young sediments which, in general, are conductive; topographic differences between the beginning and end points of profiles; the characteristics of reflection from surface objects (e.g., electrical poles, vegetation, and trees); and the orientation of GPR profiles with respect to the fault zone (profiles should be oriented perpendicular to the fault zone).

Active fault studies require detailed investigations and the main intention in such studies is to assess the field characteristics of active faults, such as their precise location, the amount of offset on the faults, and the width of deformation zones. Such parameters can easily be obtained where evidence of faulting is preserved in the geological and geomorphological records. However, regional and local conditions (e.g., sedimentation and erosion) play an important role in the preservation of surface evidence for faulting. In addition, human activities such as agriculture and construction erase the geological and geomorphological records; thus, it becomes impossible to obtain the necessary data on the field characteristics of faults from surface evidence. In these cases, alternative techniques are required to obtain essential data. The GPR method has proved to be the most flexible and useful of all the shallow geophysical methods, and it has been applied in a wide variety of disciplines,

* Corresponding author. Tel.: +90 541 502 48 93; fax: +90 286 218 05 41.
E-mail addresses: yalciner@comu.edu.tr, caglaryalciner@gmail.com (C.Ç. Yalçıner).

0264-3707/$ – see front matter © 2012 Elsevier Ltd. All rights reserved.
http://dx.doi.org/10.1016/j.jog.2012.05.011

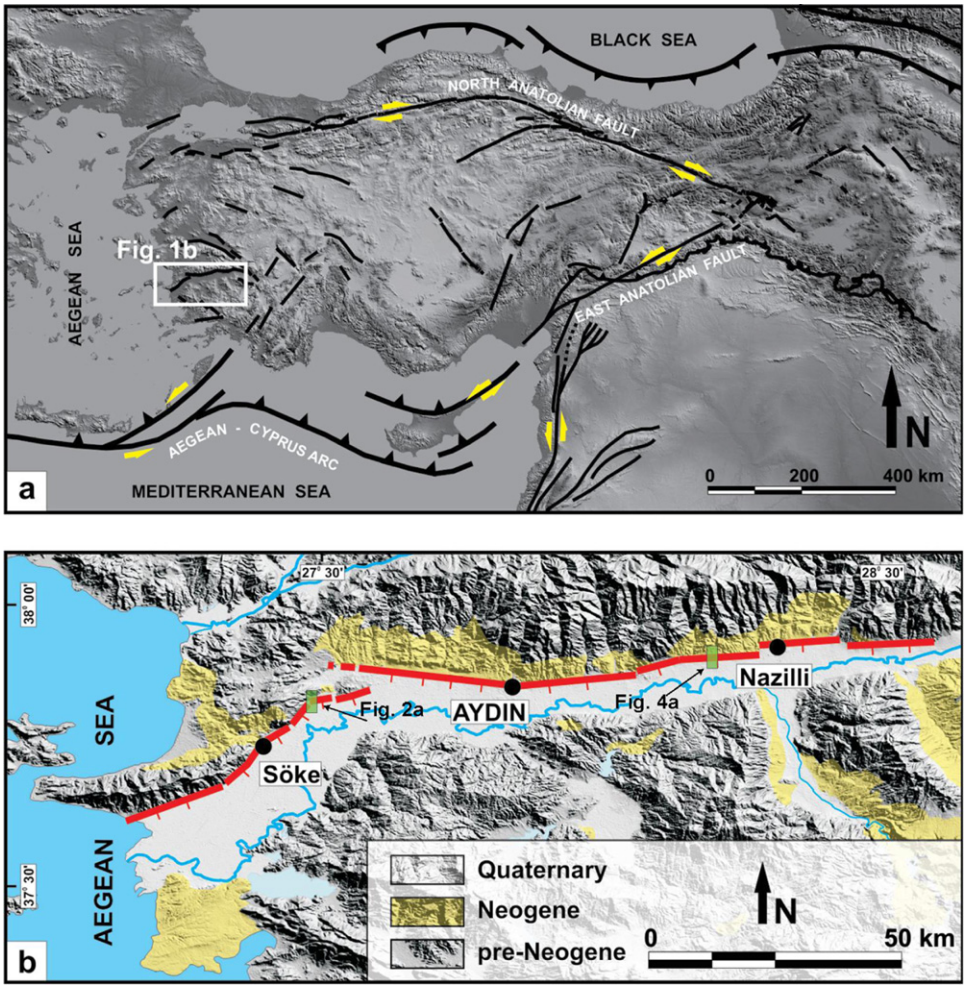

Fig. 1. (a) Map of major active tectonic structures in Turkey. (b) Simplified geological map of the Büyük Menderes Graben on shaded relief (SRTM). Red lines are the active faults along the northern side of the graben (Altunel et al., 2009). (For interpretation of the references to color in this figure legend, the reader is referred to the web version of the article.)

including active tectonic studies. For example, Bano et al. (2000) conducted GPR prospecting at a Quaternary sedimentary site to image the structures and tectonic features. Audru et al. (2001) measured three GPR profiles on an active strike-slip fault within an urban area to comprehend the geometry of the fault and minimize the impact of surface and subsurface infrastructural elements (e.g., power poles, sewers, and water mains) and traffic. Gross et al. (2002) and Green et al. (2003) applied the GPR method to investigate the location and shallow geometry of the San Andreas Fault as well as the displacement on the fault. Meghraoui et al. (2001) combined GPR investigations with electrical resistivity and seismic studies to determine precise locations for trenching. Ferry et al. (2004) identified the offset of a buried Ottoman aqueduct and stream channels on the North Anatolian Fault using GPR. Malik et al. (2007) identified shallow subsurface deformation and geometry along the Pinjore Garden Fault (NW Himalaya) using GPR. Christie et al. (2009) estimated fault displacement and off-fault deformation along the Emigrant Peak Fault (Walker Lane-Eastern California shear zone) by conducting a 3D GPR survey. Although the ability of GPR to identify buried features has been demonstrated, most investigations have been concerned with the location of buried structures. It is necessary to examine the capability of the GPR technique to estimate the amount of displacement on an active fault.

The Büyük Menderes fault zone can be easily identified in the field; it separates Holocene sediments from pre-Holocene clastic units. However, rapid erosion and modification at some locations, it is sometimes difficult to trace the fault; this is the case in locations where the fault cuts loose deposits. The Büyük Menderes Graben experienced large earthquakes in historical times (e.g., Sipahioğlu, 1979; Ambraseys and Finkel, 1995), and previous studies (e.g., Ilhan, 1971; Allen, 1975; Ambraseys, 1988; Paton, 1992; Altunel, 1999) showed that surface faulting occurred along the northern margin of the Büyük Menderes Graben. However, surface ruptures of historical events are only partly visible, either because they are covered by sediments or because of removal of the traces by erosion or man-made modifications. In this study, surface ruptures of historical earthquakes in Holocene deposits were identified and located, and the vertical displacements on the faults were estimated using GPR profiles. On the basis of GPR results, trenches were dug in the same locations, and the interpreted GPR profiles were compared with logs of the trench walls.

2. Geological and tectonic setting of the study area

The Büyük Menderes Graben is one of the principal active structures of western Turkey, which is one of the most seismically active regions of the world (Jackson and McKenzie, 1988). The width of the E–W trending Büyük Menderes Graben varies from 8 to 12 km, and mapping of geological units showed that there are three main rock associations around the Büyük Menderes Graben (e.g., Cohen et al., 1995; Emre and Sözbilir, 1995; Bozkurt, 2000). These

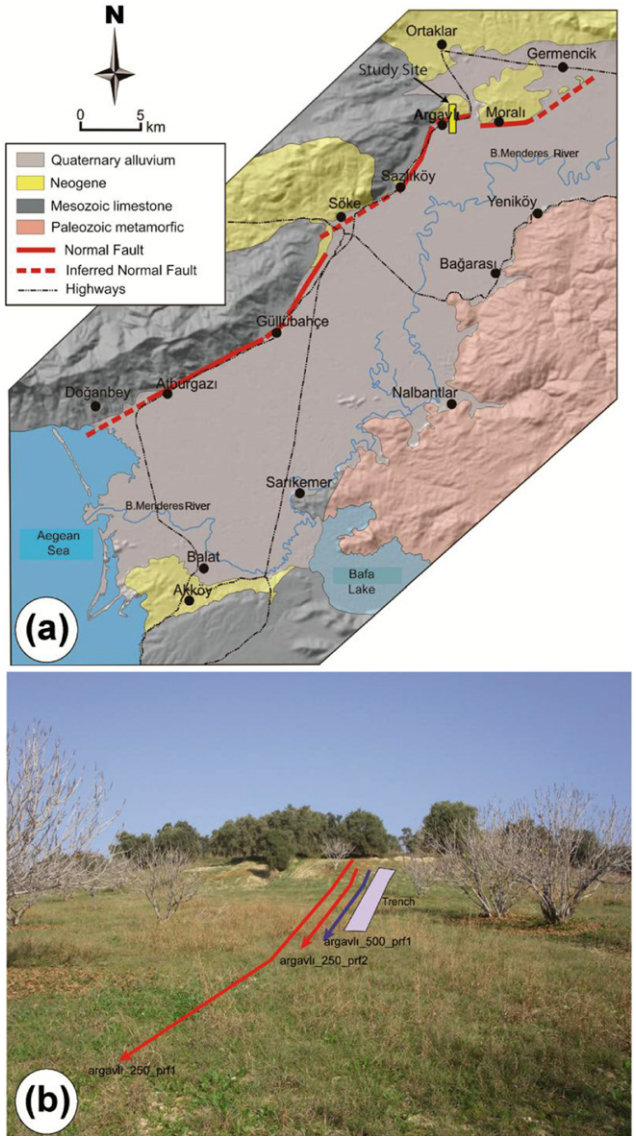

Fig. 2. (a) Detailed map of the western part of the Büyük Menderes Graben (Altunel et al., 2009). (b) View of the Argavlı site towards north. Red and blue lines are locations of GPR profiles, white rectangular box is the trench site. (For interpretation of the references to color in this figure legend, the reader is referred to the web version of the article.)

are pre-Neogene basement rocks, Neogene and Pleistocene clastic units, and Holocene deposits (Fig. 1). Pre-Neogene basement rocks include mainly marbles, schists, and limestone, cropping out along both sides of the graben (Fig. 1). Neogene–Pleistocene units consist of continental clastic sediments and crop out mainly along the northern side of the graben (Fig. 1). Holocene fluvial deposits occur mainly beneath the flat floor of the graben, while colluvial and alluvial fan sediments occur on its margins (Fig. 1). The main faults bounding the Büyük Menderes Graben are on the northern margin and this side of the graben is bounded by two sets of E–W trending south-dipping major normal faults. The northern set separates Quaternary and Neogene sediments from pre-Neogene metamorphic rocks (e.g., Emre and Sözbilir, 1995; Bozkurt, 2000; Gürer et al., 2009) (Fig. 2). The southern normal faults separate Holocene deposits from Neogene–Pleistocene units. The graben-related Neogene–Pleistocene sediments are uplifted relative to the present graben floor (Emre and Sözbilir, 1995; Koçyiğit et al., 1999; Bozkurt, 2000). Thus, as pointed out in previous studies (e.g., Paton, 1992; Emre and Sözbilir, 1995; Cohen et al., 1995; Koçyiğit et al., 1999; Altunel, 1999; Bozkurt, 2000), the southern faults are the important active structures that have ruptured during major events in the historical period and during the 20th century. Faults separating Holocene deposits from Neogene–Pleistocene units are generally expressed at the surface by prominent scarp morphology.

Table 1
Acquisition parameters of GPR survey.

Antenna freq.	500 MHz	250 MHz
Trace interval	0.05 m	0.1 m
Samples	512	512
Sampling freq.	6755 MHz	2607 MHz
Time window	76 ns	196 ns

3. GPR method and site selection

Comprehensive details of the GPR methodology are available in literature (e.g., Davis and Annan, 1989; Daniels, 2004). Ideally, GPR may provide high-resolution (up to 0.1 m) images of the subsurface over a depth range of several meters to, exceptionally, 50 m. However, the quality of the data and the depth of penetration strongly depend on the electromagnetic (EM) properties of the investigated material and the frequency range of the antennas used (Davis and Annan, 1989). Indeed, the best results have been obtained from stratified, clay-free, dry or freshwater-saturated sand or gravel (Smith and Jol, 1995).

The main objective of our study is to demonstrate the applicability of GPR imaging across normal faults and to determine its capability to complement paleoseismic trenching. A (RAMAC GPR device) was used in this study with two shielded antennas (250 MHz and 500 MHz). The 250 MHz antenna was chosen to optimize the penetration depth, vertical resolution, and survey logistics. EM wave penetration at the site was limited such that for the 250 MHz antenna, reflection events were not recorded after approximately 100 ns. Nevertheless, the 500 MHz antenna provided better resolution for low penetration depths. The acquisition parameters for both antennas are listed in Table 1.

The Büyük Menderes Graben provides a good opportunity to study the application of GPR in shallow geophysical investigations. The active Büyük Menderes fault zone can be easily traced in the field where it separates Holocene sediments from Neogene–Pleistocene units. However, in the places where the fault extends into loose Holocene deposits, it is difficult to trace it in the field because of the effects of rapid erosion or sedimentation. Hence, GPR surveys were performed in two sites with no clear surface evidence for faulting in order to precisely locate the fault zone.

The general trend of the Büyük Menderes Graben is E–W but it extends NE–SW near the Aegean Sea (Fig. 1b). The Argavlı site is located near the northeastern end of the NE–SW trending part of the graben (Fig. 2a). The active fault was mapped using geological and geomorphological indicators but its precise location in the study site was not clear because the field has been used for agriculture, which erases surface evidence of faulting. GPR surveys were applied to locate the fault precisely. The first measurements were taken with the 250 MHz antenna along an 80-m profile to obtain a general view of the subsurface (Fig. 2b). After the processing this long profile, we re-marked some offset reflectors and hyperbolas between 10 and 25 m along the profile (Fig. 3). This part of the long profile was scanned again with the 250 MHz antenna with a shorter trace interval (~5 cm) to achieve higher lateral resolution (Fig. 2b). Thereafter, we used the 500 MHz antenna for a more detailed analysis of the offset (higher vertical resolution) and for identifying different sedimentary units.

The Atça site is located on the E–W trending part of the graben between Aydın and Nazilli (Figs. 1b and 4a). A prominent morphological scarp exists between Holocene deposits and

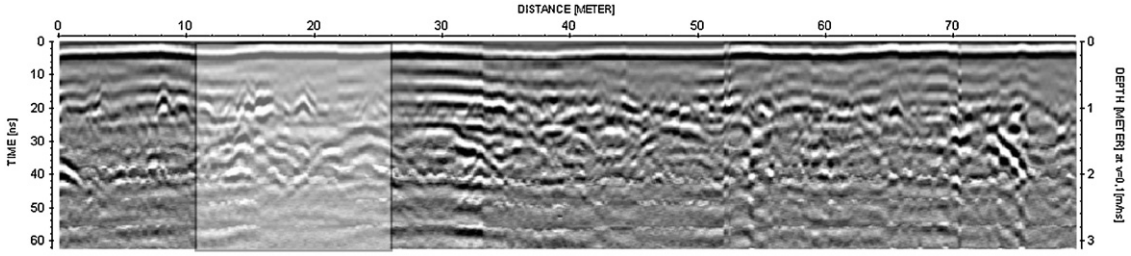

Fig. 3. GPR profile obtained with 250 MHz antenna in the Argavlı site. Gray rectangular box indicates the location of anomalous zone (vertical scale is exaggerated).

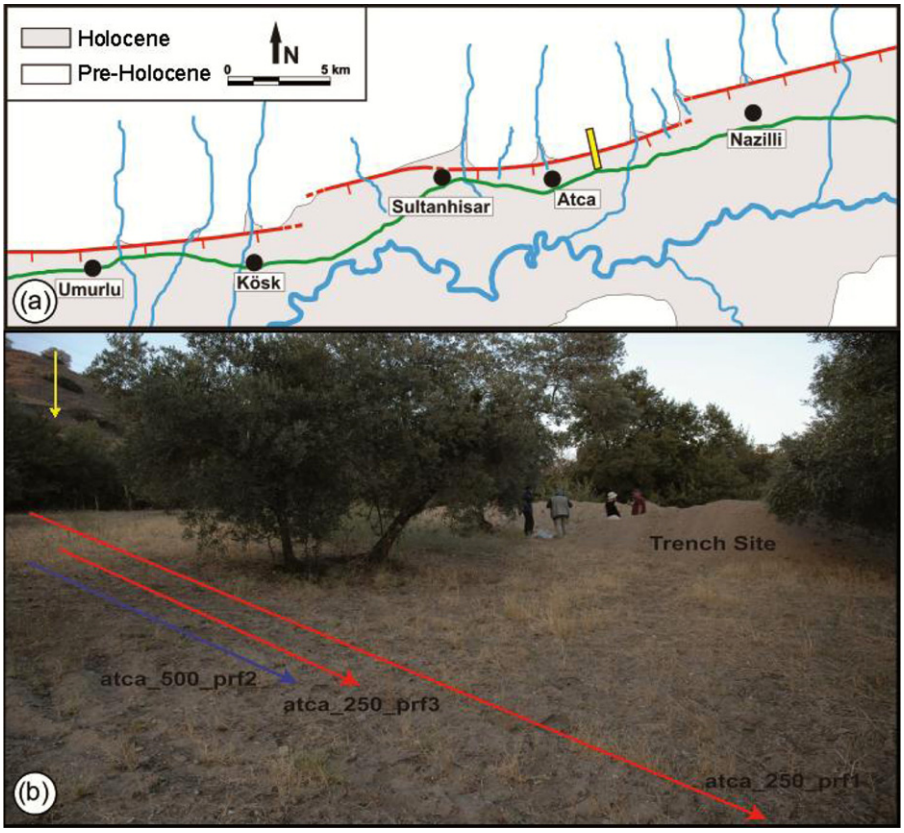

Fig. 4. (a) Simplified map of the Atça site showing geological units and active faults (Altunel et al., 2009). Yellow rectangular box indicates study site. (b) View of the Atça site towards north. Note morphological scarp in pre-Quaternary deposits (yellow arrow). (For interpretation of the references to color in this figure legend, the reader is referred to the web version of the article.)

Neogene–Pleistocene units about 2 km east of the town of Atça (Fig. 4b). This scarp built up as a result of the uplifting of the Neogene–Pleistocene units on the northern side. However, there is a gentle slope in the Holocene deposits about 10 m south of this scarp (Fig. 4b). In order to clarify whether this gentle morphological scarp in the Holocene deposits reflects the location of recent faulting, we obtained GPR profiles of this location. First, the site was scanned with a 250 MHz antenna from the foot of the high scarp to the end of the field across the gentle morphological scarp (Fig. 4b). On processing this ~50-m long profile, offset reflectors and hyperbolas were observed between 34 and 36 m along the profile (Fig. 5); this interval coincides with the gentle scarp in Holocene deposits.

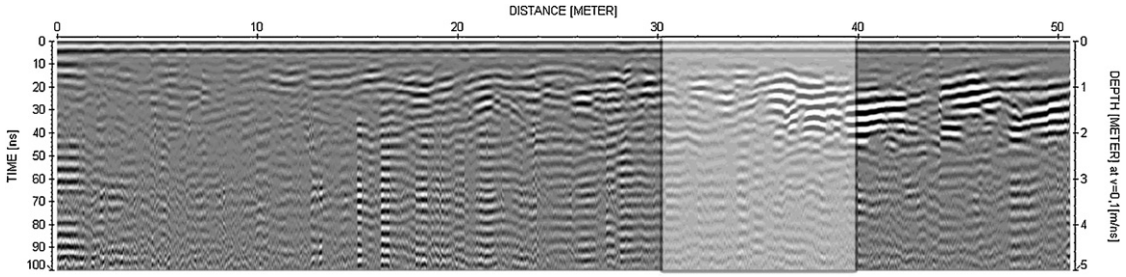

Fig. 5. GPR profile obtained with 250 MHz in the Atça site. Highlighted area indicates location of the peculiar zone (vertical scale is exaggerated).

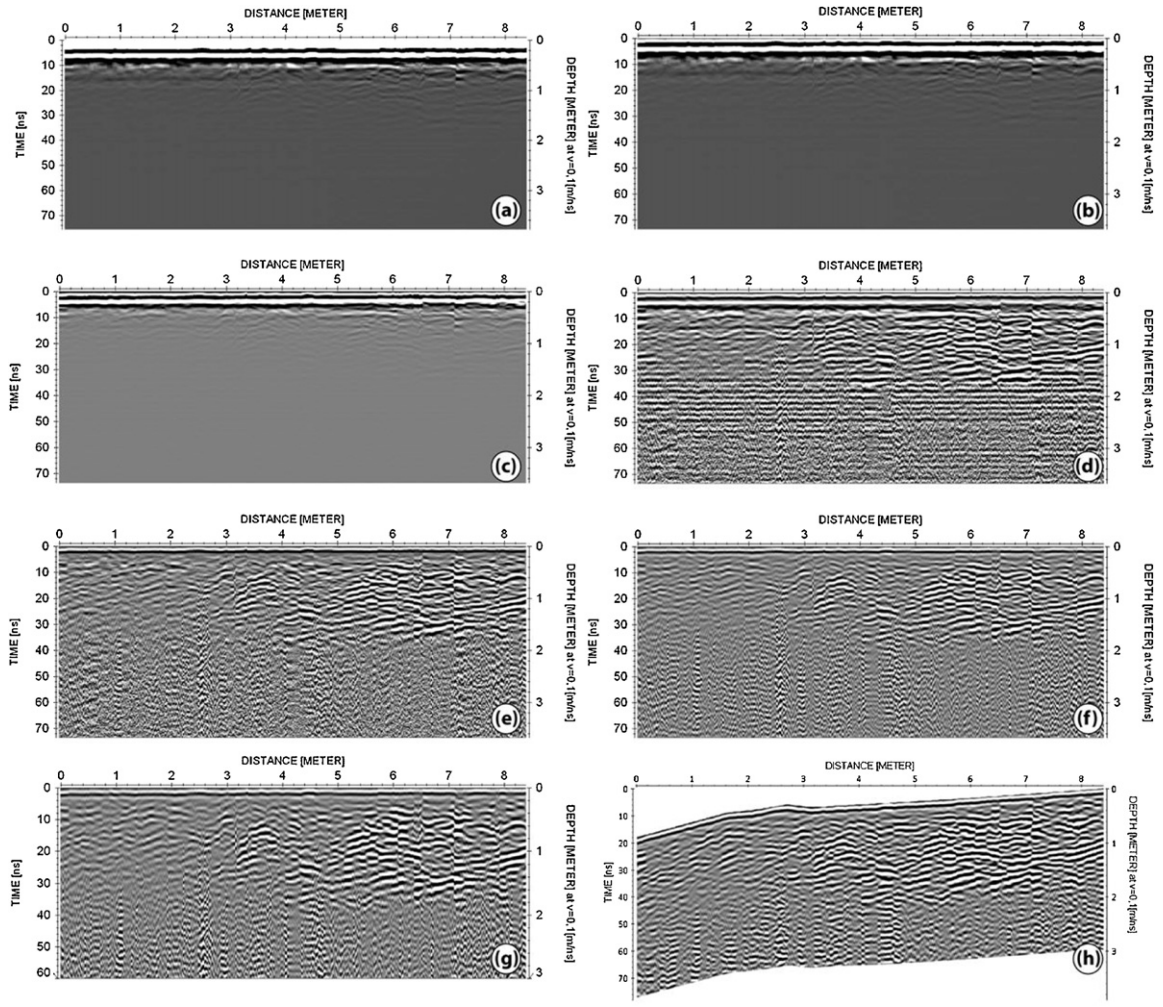

Fig. 6. Processing steps of a GPR profile (500 MHz) from Atça site, (a) raw data, (b) constant time shift correction, (c) DC filtering with subtract-mean (dewow), (d) gain application with energy decay, (e) filtering of flat coherent noise with subtracting average trace, (f) band-pass filtering, (g) time cut filtering, (h) application of topographic corrections.

After recognizing this anomaly, detailed measurements were taken with the 250 and 500 MHz antennas over a short distance.

4. Results of field studies

The raw GPR data have to be appropriately processed in order to interpret the data. Commercially available Reflex W (Sandmeier, 2003) software was used for processing the data. Each profile was processed as follows (see Fig. 6):

a. Raw data (Fig. 6a).
b. Move start-time (manual input): ~2 ns for 500 MHz, ~6 ns for 250 MHz (Fig. 6b).
c. DC (direct current) filtering by subtract-mean (dewow): 2 ns window for 500 MHz data, and 4 ns window for 250 MHz data (Fig. 6c).
d. Energy decay curve: scaling value 0.512 (Fig. 6d).
e. Subtracting average trace in order to remove flat coherent noise: 31 traces for 250 MHz data, and 31–61 traces for 500 MHz data, start time: 3–6 ns (Fig. 6e).
f. Band-pass filtering: 200/400–600/800 for 500 MHz data, and 100/200–300/400 for 250 MHz data (Fig. 6f).
g. Time cut: 60 ns for 500 MHz data, 60 ns for 250 MHz data (in Argavlı site), and 100 ns for 250 MHz data (in Atça site) (Fig. 6g).
h. Topographic correction (Fig. 6h).

4.1. Argavlı site

4.1.1. GPR results

Fig. 7 shows the processed and interpreted data of the 250 MHz GPR profile in the Argavlı site. The 250 MHz antenna does not provide good vertical resolution but shows clear continuous flat reflectors for layering. From the interpreted profile (Fig. 7b), 5 different lithological units were identified (Fig. 7b). It is clear that there are three deformation zones between 3 and 11 m along the profile. Some vertical displacements can be recognized in the interpreted profile, but the error in the vertical resolution is about ±10 cm for the 250 MHz antenna. Thus, estimate of vertical displacements from the 250 MHz GPR profile would not be reliable.

The 500 MHz antenna was used on the same profile to obtain a better vertical resolution because the error in the vertical resolution is about ±5 cm. The 500 MHz shielded antenna yielded satisfactory results; on processing, the profile showed clearer reflectors and hyperbolas (Fig. 8a). The units recognized with the 250 MHz antenna are much clearer in the 500 MHz profile (Fig. 8a and b).

The units identified in the interpreted profile are marked as A–G in Fig. 8b. The deformation zone is much clearer, and four different faults (F_1–F_4) can be recognized between 3 and 9 m along the profile (Fig. 8b). Unit A is ploughed soil and all units beneath this

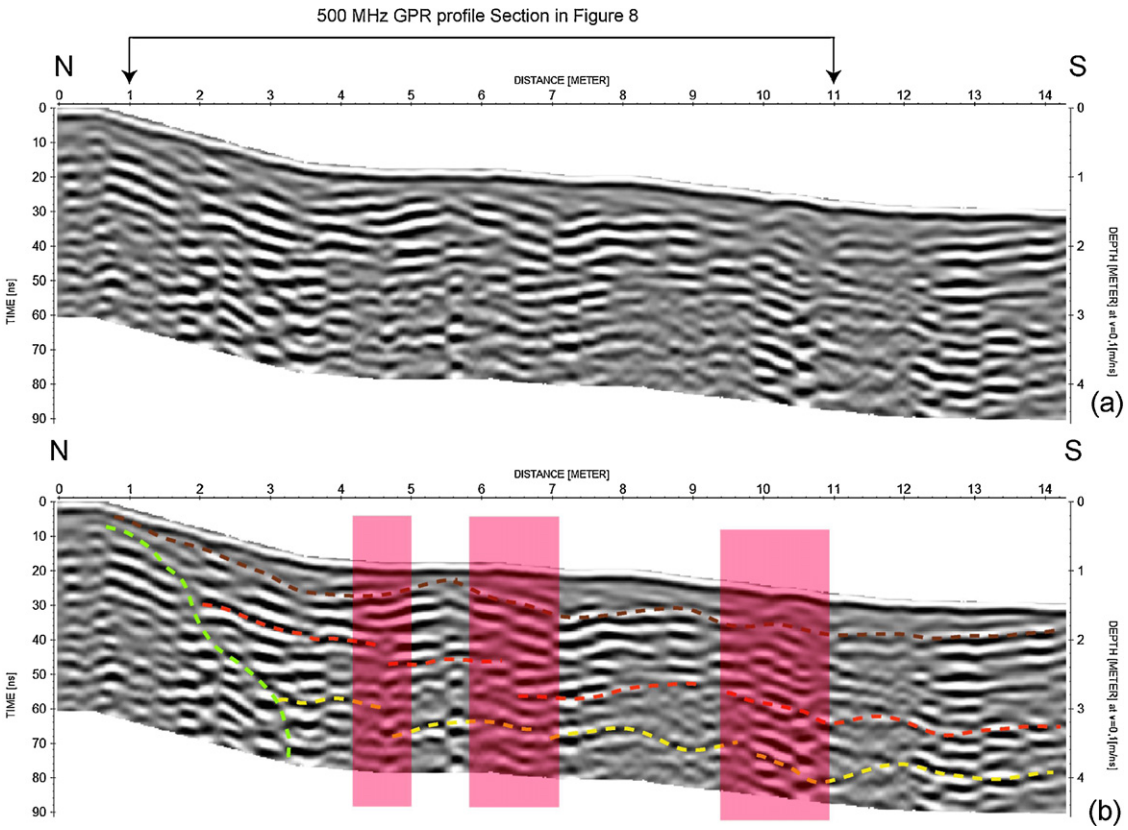

Fig. 7. 250 MHz GPR profile in the Argavlı site. (a) Processed profile. (b) Interpreted profile. Dashed lines represent the interfaces; highlighted areas (red boxes) represents deformation zones. (For interpretation of the references to color in this figure legend, the reader is referred to the web version of the article.)

level are offset by the four faults. The interpreted profile from the 500 MHz antenna showed the following: fault F_1 causes ~80 cm vertical offset of units C–E; fault F_2 vertically offsets units D and E by ~30 cm; fault F_3 causes ~30 cm vertical offset of units C–E; and fault F_4 vertically offsets units B–E by ~20 cm. The interpreted profile also shows that while faults F_1, F_2, and F_3 are covered by soil, F_4 terminates at about 1 m depth.

4.1.2. Trench results

Following the GPR studies, a 13-m-long and 2.5-m-deep trench was dug across the identified fault zone. Fig. 8c shows the log of the eastern trench wall, where 9 units were exposed, including silt, sand, and pebbles. Six main faults were recognized within a 7-m-wide deformation zone in the trench (Fig. 8c). Vertical offset is ~80 cm on fault f_1, ~30 cm on fault f_2, ~30 cm on fault f_3, ~20 cm on fault f_4, ~15 cm on fault f_5, and ~30 cm on fault f_6. Fault f_3 extends up to the recent soil but the other faults ends at different depths (Fig. 8c).

4.2. Atça site

4.2.1. GPR results

Fig. 9a shows the GPR profile of the Atça site taken with the 250 MHz antenna. Five different levels can be identified in the processed profile (Fig. 9b). Disturbances of GPR reflectors between 4 and 7 m along the profile are interpreted as deformation zones. Thus, the 500 MHz antenna was used along the same line to achieve better resolution (Fig. 10a).

Interpretation of the processed 500 MHz GPR profile clearly shows eight different stratigraphic levels and two faults (Fig. 10b). Tabular reflectors in the upper northern part of the profile are interpreted as channel deposits (C in Fig. 10b). The 500 MHz profile provides vertical resolution good enough to estimate vertical offsets on faults. The vertical offset is about 80 cm on fault F_1 and about 50 cm on fault F_2 (Fig. 10b).

4.3. Trench results

Following the GPR interpretation, a 13-m-long and 3.5-m-deep trench was dug across the identified fault zone (Fig. 10b). Detailed logging of the western trench wall showed nine different units, channel deposits, and four faults (Fig. 10c). Faults f_1–f_3 are single branches and they end about 1.5 m below the surface, but fault f_4 is a shear zone and reaches up to the recent soil. The total vertical offset is about 3.5 m on fault f_4 but about 50 cm on each of f_1–f_3 faults.

5. Comparison of GPR profiles with trench logs and discussion

Reactivation of the Büyük Menderes Graben fault resulted in surface-rupturing earthquakes in historical times (Ilhan, 1971; Allen, 1975; Sipahioğlu, 1979; Ambraseys, 1988; Paton, 1992; Altunel, 1999). Surface ruptures of historical earthquakes are partly visible along the northern side of the graben but most evidence for faulting no longer exists, either as a result of geological processes (erosion and sedimentation) or of man-made activity. The GPR method provided useful results, and we were able to identify the precise location of the most recent buried normal fault zone at two sites – Argavli (Fig. 2a) and Atça (Fig. 4a). In addition, the vertical displacement on each fault branch was estimated from disturbed reflectors on GPR profiles before trenching.

The Argavlı site is located in the western part of the graben where faults trend NE–SW (Figs. 1b and 2a). Fig. 8b and c shows the

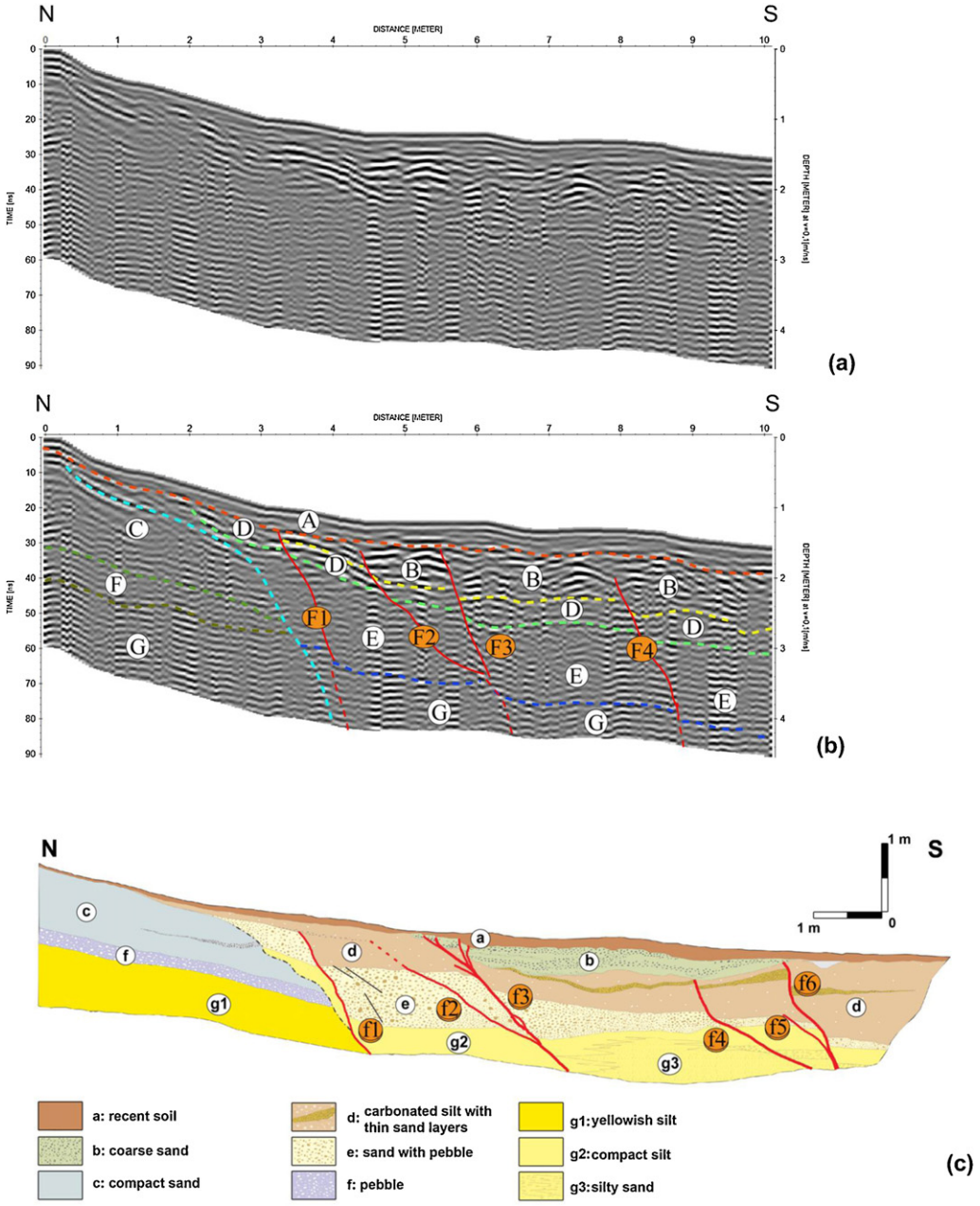

Fig. 8. Comparison of the 500 MHz GPR profile with the trench log in the Argavlı site. (a) Processed profile. (b) Interpreted profile. Dashed lines represent interfaces, letters from "A" to "G" show different layers, red lines represent possible faults. (c) Log of Argavlı trench (eastern wall), f_1–f_6 are main faults. All figures are in the same scale and there is no vertical exaggeration. (For interpretation of the references to color in this figure legend, the reader is referred to the web version of the article.)

interpreted 500 MHz GPR profile and the trench log of the Argavlı site, respectively. Different units in GPR profiles were identified from top to bottom considering the positive to negative transition in signal amplitude after processing. Some flat reflectors that are assigned as unit boundaries (such as the lower boundaries of units D and E) display interruptions, but trace-by-trace investigation showed similar positive to negative transition in signal amplitude. Thus, they are considered to be contacts between two units. By considering the transition line as the lower contact of a unit, seven different units can be identified in the interpreted GPR profile (Fig. 8b). The penetration depth of the GPR is not enough to identify the lower contact of the base units below units E and F in the GPR profile. Thus, this part of the profile is shown as the same unit (unit G). However, the trench wall exposed nine units (Fig. 8c). Unit A is the recent soil, both in the GPR profile and in the trench log. Units B–F in the GPR profile can be correlated with the same units in the trench exposure. Unit G in the GPR profile represents units g1–g3 in the trench wall.

The Atça site is located on the E–W trending part of the graben (Fig. 4a). Eight different units and some channel deposits were identified in the interpreted GPR profile (Fig. 10b) but the trench log showed nine different units and eight channel deposits (Fig. 10c). There is recent soil (unit A) at the top of GPR profile and trench log. Unit C comprises channel deposits in both the GPR profile and the trench log, and the deposits were identified by their shapes in the GPR profile (Fig. 10b). Units B–G in the GPR profile can be correlated with the same units in the trench exposure. Units h and i in the trench wall interfere with channel deposits and these two units were identified as a single unit (unit H) in the GPR profile.

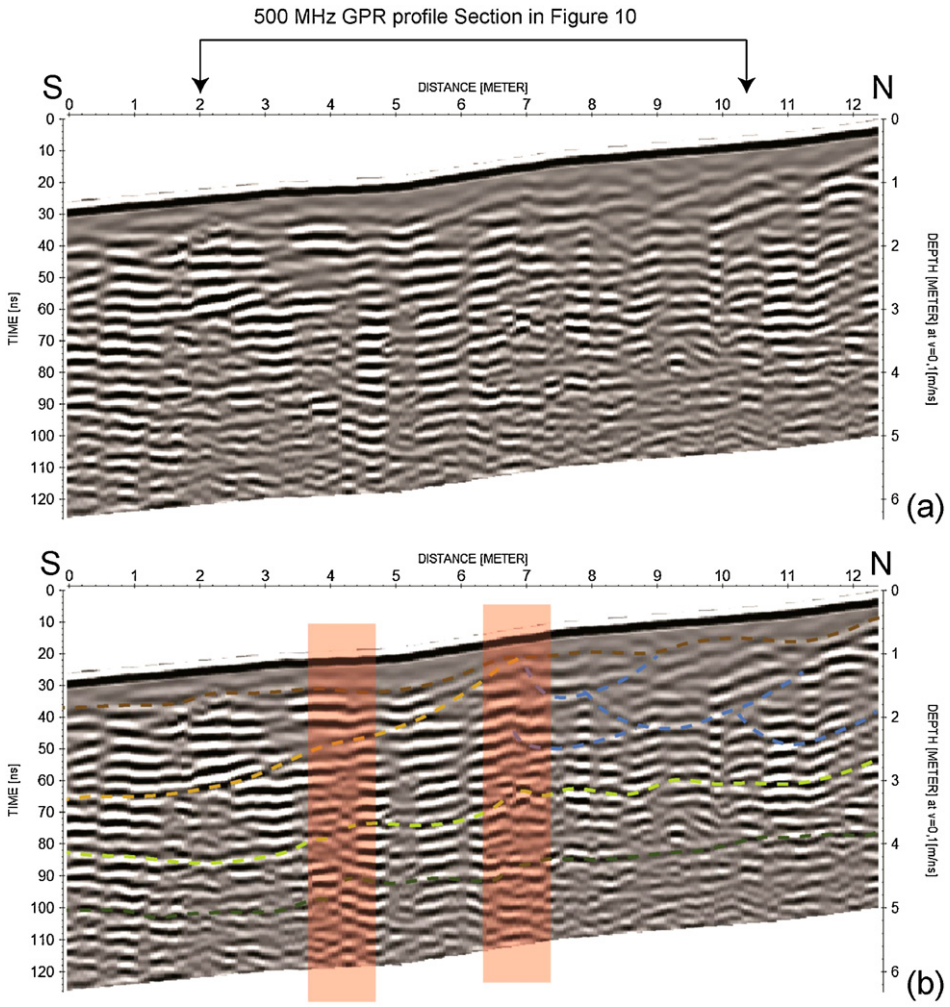

Fig. 9. 250 MHz GPR profile in Atça site. (a) Processed profile. (b) Interpreted profile. Dashed lines represent different layers, highlighted areas (red boxes) represents deformation zones. (For interpretation of the references to color in this figure legend, the reader is referred to the web version of the article.)

Although units in the interpreted GPR profiles can be correlated with the trench exposure, width and depth of units varies, probably due to the antenna resolution. In addition, more separate units are exposed in the trench log. The trench walls were logged directly by observation; thus, a single lithological unit can be divided in different sub-units on the basis of content, texture, and structure of sediments. However, considering the contrast of the dielectric constants of different units in GPR profiles, GPR prospecting allows only the gross identification of main lithological units. Therefore, the number of recognized units in GPR profiles (Figs. 8b and 10b) is less than the number of observed units in trench walls (Figs. 8c and 10c). Similarly, the recognition of channel fills in the GPR profile is related to the grain size and, probably, the humidity content. This is likely the main reason we have observed more channel fills in the trench log than in the GPR data.

Flat reflectors between two different units were considered to identify faults in the GPR profile. Interruptions to these flat reflectors were interpreted as faults. Roughness on the surface, roots, or change in antenna orientation with respect to the ground may also cause variations in the recorded reflections that can be confused with real changes in the ground (Conyers, 2004; Yalçıner et al., 2009). Such undesirable effects usually display straight vertical interruptions, which do not cause displacements in flat reflectors. Flat reflectors were examined trace-by-trace to eliminate unnatural disruptions. Based on displaced reflectors in the GPR profiles, we identified main faults in the studied sites. The interpreted profile suggests four south facing main faults in the Argavlı site (Fig. 8b). Faults F_1 and F_2 terminate about 40 cm and 50 cm below the surface, respectively, while fault F_3 ends at about 50 cm depth and F_4 ends at about 80 cm depth (Fig. 8b). Trench logs show two additional faults in the Argavlı site that are not visible in the GPR profile (Fig. 7b). The vertical offsets on faults f_5 and f_6 are 10 cm and 30 cm, respectively. The likely reason why faults f_5 and f_6 were not recognized in the GPR profile is that the vertical resolution (that depends on the used frequency/wavelength) of the 250 MHz antenna is probably less than the vertical resolution observed directly on the trench walls. Since faults f_5 and f_6 were not recognized in the 250 MHz GPR profile, the southern part was not scanned further with the 500 MHz antenna. It is noteworthy that the positions of the recognized faults in the interpreted GPR profile (Fig. 8c) are consistent with those in the trench log.

The interpreted GPR profile suggests two south facing main faults in the Atça site (Fig. 10b). Fault F_1 is a single line that terminates about 1.5 m below the surface and fault F_2 is branching-upward and terminates about 40 cm below the surface (Fig. 10b). The trench log shows four faults at this site (Fig. 10c). Faults F_1 and F_2 in the GPR profile probably correspond with faults f_2 and f_4 in the trench log, respectively. Faults f_1 and f_3 in the trench log were not recognized in the GPR profile, probably due to the lithology of the offset units. GPR and trench studies at this site showed that recent faulting had occurred in Holocene deposits and does not follow the present morphology of the scarp that is about 10 m north of the site

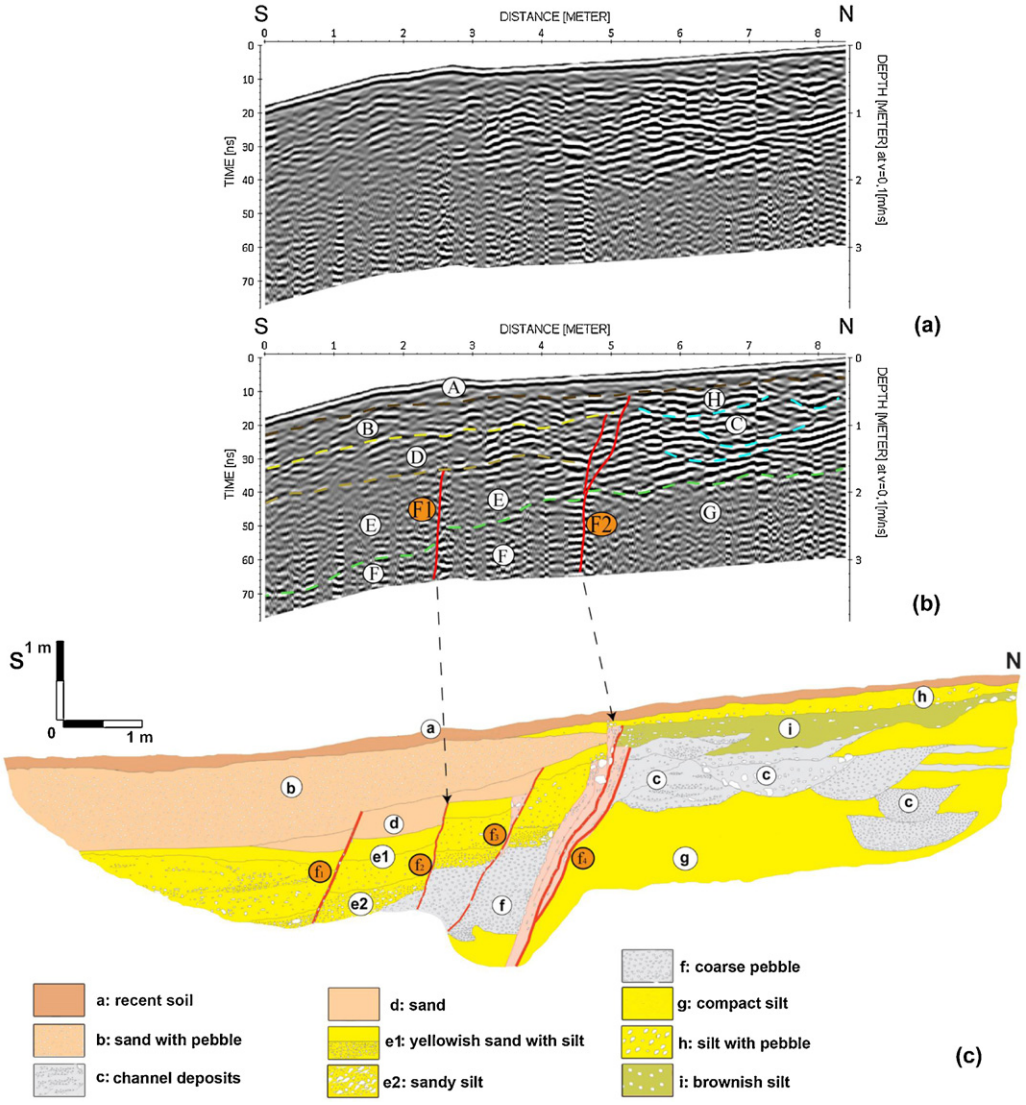

Fig. 10. Comparison of the 500 MHz GPR profile with the trench log in the Atça site. (a) Processed profile. (b) Interpreted profile. Dashed lines represent five different interfaces and the letters from "A" to "H" represent different layers, red lines represent possible faults. (c) Log of Atça trench, western wall, f_1–f_4 are main faults. All figures are in the same scale and there is no vertical exaggeration. Unit "F" exposes below unit "E" in both sides of the fault F1 in GPR profile (Fig. 10b) but the same unit cannot be seen in the trench log because the trench is not as deep as the GPR profile in this part (GPR profile is about 3 m, trench is about 2.5 m in this part). (For interpretation of the references to color in this figure legend, the reader is referred to the web version of the article.)

(Fig. 4b). The location of this faulting in Holocene deposits suggests that faulting propagates towards the basin, something that was previously observed by Cohen et al. (1995) in the Büyük Menderes Graben. Nevertheless, without performing GPR, field observations alone in this location would not be capable of recognizing the fault propagation towards the basin.

Although the interpreted GPR profiles in both the Argavlı and Atça sites are consistent with the trench logs, fault dips are greater in the GPR profiles (Figs. 8b and 10b). This difference is probably related to the following factors: (1) the GPR profiles are not strictly perpendicular to the fault strike at depth, and (2) a simple topographic correction was carried out for each profile trace-by-trace using a constant EM velocity but migration was not applied to the GPR data.

Identification of the boundaries of main lithological units in GPR profiles would permit estimation of the total amount of offset on faults. Thus, we tried to estimate the amount of cumulative offset for each fault from the GPR profiles and compared the results with direct observations from trench logs. Table 2 compares estimated offsets (from Argavlı GPR profiles) with measured offsets (in the Argavlı trench log). We notice that the results are comparable and quite consistent for each fault.

Table 2
Amount of offsets recognized in Argavlı GPR profiles and observed in trench log.

Fault	Estimated offset (from GPR)	Measured offset (trench wall)
fi	~80 cm ± 7 cm	~80 cm
fii	~30 cm ± 7 cm	~30 cm
fiii	~30 cm ± 7 cm	~30 cm
fiv	~20 cm ± 7 cm	~20 cm
fv	?	~10 cm
fvi	?	~30 cm

6. Conclusions

The observation of surface ruptures along the northern flank of the Büyük Menderes Graben was difficult and very limited in terms of visibility, mostly because of erosion, sedimentation, and human activity. To complement field observations of fault scarps,

we performed GPR prospecting in areas where the main fault segment is buried and no visual account of the precise location of the fault is available. Field observations alone would not be capable of recognizing these fault traces.

The main fault segment in the Argavlı site separates Holocene deposits from Neogene units. In the Atça site, previous studies interpreted the abovementioned scarp (which is clearly traceable between Neogene and Pleistocene units and Holocene deposits) as the location of active faults. However, GPR interpretation combined with trench studies showed that the current active, and probably seismogenic, fault trace developed within Holocene deposits at the Atça site.

The GPR and trench studies that we have conducted in the Büyük Menderes Graben produced striking results, especially in regions with suitable geological (dry and clay-free) and geomorphological (low inclination) conditions. Therefore, in regions where trench excavations are not possible, GPR surveys might provide important information on the characteristics of active faults.

Acknowledgements

This research is supported by TUBITAK (105Y348), Research Foundation of Eskişehir Osmangazi University (200415001, 200615026) and CNRS-UMR 7516 Strasbourg. The first author (C.Ç. Yalçıner) has been supported during his PhD by a "cotutelle" scholarship from Embassy of France in Turkey. We thank Ziyadin Çakır for his critical reviews and suggestions that greatly improved the paper. We also thank to Önder Yönlü for his help in the field. We are really grateful for helpful comments and constructive reviews by anonymous reviewers which improved our manuscript.

References

Allen, C.R., 1975. Geologic criteria for evaluating seismicity. Geological Society of America Bulletin 86, 1041–1056.

Altunel, E., 1999. Geological and geomorphological observations in relation to the 20 September 1899 Menderes earthquake, Western Turkey. Journal of the Geological Society, London 156, 241–246.

Altunel, E., Akyüz, H.S., Meghraoui, M., Kiyak, N.G., Karabacak, V., Yalçıner, C.Ç., 2009. Archeoseismology and Paleoseismology of the Büyük Menderes fault zone, Project report (TÜBİTAK Project No. 105Y348). p. 205 (unpublished).

Ambraseys, N.N., 1988. Engineering seismology. Earthquake Engineering and Structural Dynamics 17, 1–105.

Ambraseys, N.N., Finkel, C.F., 1995. Türkiye'de ve komşu bölgelerde sismik etkinlikler. Bir Tarihsel İnceleme 1500-1800. TÜBİTAK Yayınları Akademik Dizi-4.

Annan, A.P., Waller, W.M., Strangway, D.W., Rossiter, J.R., Redman, J.D., Watts, R.D., 1975. The electromagnetic response of a low-loss, 2-layer dielectric earth for horizontal electric dipole excitation. Geophysics 40 (2), 285–298.

Audru, J.-C., Bano, M., Begg, J., Berryman, K., Henrys, S., Niviere, B., 2001. GPR investigations on active faults in urban areas: the Georisc-NZ project in Wellington, New Zealand. Earth and Planetary Science 333 (8), 447–454.

Bano, M., Marquis, G., Nivière, B., Maurin, J.-C., Cushing, M., 2000. Investigating alluvial and tectonic features with ground-penetrating radar and analysing diffraction patterns. Journal of Applied Geophysics 43, 33–41.

Bano, M., Loeffler, O., Girard, J.-F., 2009. GPR response and FDTD modeling to fuel infiltration in a sand box experiment. Comptes Rendus Geoscience 341, 846–858.

Bozkurt, E., 2000. Timing of extension on the Büyük Menderes graben, Western Turkey, and its tectonic implications. Geological Society London, Special Publications 173, 385–403.

Christie, Tsoflias, M.G.P., Stockli, D.F., Black, R., 2009. Assessing fault displacement and off-fault deformation in an extensional tectonic setting using 3-D ground-penetrating radar imaging. Journal of Applied Geophysics 68 (1), 9–16.

Cohen, H.A., Dart, C.J., Akyüz, H.S., Barka, A., 1995. Syn-rift sedimantation and structural development of the Gediz and Büyük Menderes graben, Western Turkey. Journal of the Earth Society, London 152, 629–638.

Conyers, L.B., 2004. Ground-penetrating Radar for Archaeology. Altamira Press, Walnut Creek, California.

Daniels, D.J., 2004. Ground Penetrating Radar, 2nd ed. Iee Radar, Sonar, Navigation and Avionics Series, London, United Kingdom.

Davis, J.L., Annan, A.P., 1989. Ground penetrating radar for high resolution mapping of soil and rock stratigraphy. Geophysical Prospecting 37, 531–551.

Emre, T., Sözbilir, H., 1995. Field evidence for metamorp-hic core complex detachment faulting and accommo-dation faults in the Gediz and Büyük Menderes gra-bens (West Turkey): International Earth Sciences Colloquium on Aegean Regions, Izmir, Program and Abstracts, p. 15.

Ferry, M., Meghraoui, M., Girard, J.-F., Rockwell, T.K., Kozaci, Ö., Akyuz, S., Barka, A., 2004. Ground-penetrating radar investigations along the North Anatolian fault near Izmit. Geology 32 (1), 85–88.

Green, A., Gross, R., Holliger, K., Horstmeyer, H., Baldwin, J., 2003. Results of 3-D georadar surveying and trenching the San Andreas fault near its northern landward limit. Tectonophysics 368, 7–23.

Gross, R., Green, A., Holliger, K., Horstmeyer, H., Baldwin, J., 2002. Shallow geometry and displacements on the San Andreas fault near Point Arena based on trenching and 3D georadar surveying. Geophysics Research Letter 29, 34-1–34-4.

Gürer, Ö.F., Filoreau, N.S., Özburan, M., Sangu, E., Doğan, B., 2009. Progressive development of the Büyük Menderes graben based on new data, Western Turkey. Geological Magazine 146 (5), 652–673.

Ilhan, E., 1971. Earthquakes in Turkey. In: Campbell, A.S. (Ed.), Geology and History of Turkey. Petroleum Exploration Society of Libya, pp. 431–442.

Jol, H.M., 1995. Ground penetrating radar antennae frequencies and transmitter powers compared for penetration depth, resolution and reflection continuity. Geophysical Prospecting 43, 693–709.

Jackson, J., McKenzie, D.P., 1988. The relationship between plate motions and seismicmoment tensors, and the rates of active deformation in the Mediterranean and Middle East. Geophysical Journal of Royal Astronomical Society 93, 45–73.

Koçyiğit, A., Yusufoğlu, H., Bozkurt, E., 1999. Discussion on evidence from the Gediz Graben for episodic two-stage extension in Western Turkey. Journal of the Geological Society 156, 1240–1242.

Lalumiere, L., 2000. Helicopter Hard-mounted Tests of Commercially Available GPR Systems for Snow and Ice Thickness Measurement. Internal Report for DSS contract F5955-09-0375.

Lalumiere, L., 2006. Ground penetrating radar for helicopter snow and ice surveys. Canadian Technical Report of Hydrography and Oceans Sciences, 248.

Leckebusch, J., 2003. Ground-penetrating radar: a modern three-dimensional prospection method. Archaeological Prospection 10, 213–240.

Leucci, G., Negri, S., 2006. Use of ground penetrating radar to map subsurface archaeological features in an urban area. Journal of Archaeological Science 33, 502–512.

Malik, J.N., Sahoo, A.K., Shah, A.A., 2007. Ground-penetrating radar investigation along Pinjore Garden Fault: implication toward identification of shallow subsurface deformation along active fault, NW Himalaya. Current Science 93 (10), 1427–1442.

Meghraoui, M., Camelbeeck, T., Vanneste, K., Brondeel, M., Jongmans, D., 2001. Active faulting and paleoseismology along the Bree fault, lower Rhine graben, Belgium. Journal of Geophysical Research 105 (B6), 13,809–13,841.

Paton, S., 1992. Active normal faulting, drainage patterns and sedimentation in southwestern Turkey. Journal of the Geological Society of London 149, 1031–1044.

Sandmeier, K.J., 2003. Reflex W 4.2 Manuel Book. Sandmeier Software. Zipser Strabe 1, D-76227 Karlsruhe, Germany.

Scambos, T., Bauer, R., 2006. GPR and GPS Data: Characteristics of Snow Megadunes and their Potential Effect on Ice Core Interpretation. National Snow and Ice Data Center. Digital media, Boulder, CO, USA.

Sipahioğlu, S., 1979. Büyük Menderes açılımı ile Menderes Masifi yükselminin sınırını oluşturan kuşağa uygulanan bir deprem öncesi çalışma. Deprem Araştırma Enstitüsü Bülteni 25, 5–27.

Smith, D.G., Jol, H.M., 1995. Ground penetrating radar: antenna frequencies and maximum probable depth soft penetration in Quaternary sediments. The Journal of Applied Geophysics 33, 93–100.

Yalçıner, C.Ç., Bano, M., Kadıoğlu, M., Karabacak, V., Meghraoui, M., Altunel, E., 2009. New temple discovery at the archaeological site of Nysa (western Turkey) using GPR method. Journal of Archaeological Science 36 (8), 1680–1689.